



Diketopyrrolopyrrole based small molecules with near infrared absorption for solution processed organic solar cells



Huijing Zhang^{a, b}, Nailiang Qiu^{a, b}, Wang Ni^{a, b}, Bin Kan^{a, b}, Miaomiao Li^{a, b}, Qian Zhang^{a, b}, Xiangjian Wan^{a, b, *}, Yongsheng Chen^{a, b, **}

^a State Key Laboratory and Institute of Elemento-Organic Chemistry, Collaborative Innovation Center of Chemical Science and Engineering (Tianjin), School of Materials Science and Engineering, Nankai University, Tianjin 300071, China

^b Key Laboratory of Functional Polymer Materials and the Centre of Nanoscale Science and Technology, Institute of Polymer Chemistry, College of Chemistry, Nankai University, Tianjin 300071, China

ARTICLE INFO

Article history:

Received 15 September 2015
Received in revised form
24 November 2015
Accepted 25 November 2015
Available online 14 December 2015

Keywords:

Small molecule
Organic solar cell
Diketopyrrolopyrrole
Near infrared absorption
Low band gap
Additive

ABSTRACT

Two small molecules DOR2TDPP and DCAO2TDPP with a diketopyrrolopyrrole (DPP) unit as the central building block have been designed and synthesized for solution-processed bulk-heterojunction (BHJ) solar cells. The two molecules in films exhibited broad absorption ranging from 300 to 900 nm with optical bandgaps of around 1.40 eV. The BHJ solar cell devices based on the DOR2TDPP and DCAO2TDPP as donors and PC₇₁BM as acceptors gave a PCE of 2.05% and 1.09%, respectively, under the illumination of AM.1.5G, 100 mW cm⁻². The influence of blend ratio of donor/acceptor and amount of additive on the performance of the solar cell were studied systematically.

© 2015 Elsevier Ltd. All rights reserved.

1. Introduction

Organic solar cells (OSCs) have attracted great attentions due to the potential advantages such as low cost, flexibility and etc. In contrast to the widely studied polymer based OSCs, small molecular organic solar cells (SM-OSCs) demonstrated many outstanding advantages, such as well-defined structure and definite molecular weight, easiness to purification, and thus little batch-to-batch variation. Recently, the power conversion efficiency (PCE) of ~10% [1–3] has been achieved for SM-OSCs, indicating that the PCE of SM-OSCs could be indeed comparable with that of polymer solar cells [4–11] and even higher PCEs could be expected for SM-OSCs through combination of delicate molecule design and device

optimization. The PCE of OSC are determined by three parameters, open circuit voltage (V_{oc}), short circuit current density (J_{sc}) and fill factor (FF). Generally, SM-OSCs have a high V_{oc} and FF over 70% have also been achieved for many SM-OSCs. So, to improve the J_{sc} without sacrificing the V_{oc} and FF is one of the effective strategies to get high PCE for OSCs. There are many methods to improve the J_{sc} , such as active layer morphology controlling by adding additives [12–14], thermal annealing [15], solvent vapor annealing [16,17], modification of buffer layer [18], applying anti-reflection coating [19,20], and so on. In fact, the direct and fundamental strategy to improve the J_{sc} is to design new donor molecules with broad light absorption range and high harvest efficiency.

The diketopyrrolopyrrole (DPP) unit, as a well known dye unit with many excellent properties such as strong light absorption, photochemical stability, good charge carrier mobility and etc., have been widely used not only in polymers based OSCs but also in SM-OPVs. In 2009, a DPP unit based molecule was reported with a PCE of 4.4%, which was the highest PCE in the field of solution processed SM-OSCs at that time [21]. Nowadays, various DPP based small molecules have been designed [22]. All of them have symmetric molecule structures, in which the DPP unit serves as the central core or end unit. Recently, our group have reported series of donor molecules with an acceptor-donor-acceptor (A-D-A) structure and

* Corresponding author. State Key Laboratory and Institute of Elemento-Organic Chemistry, Collaborative Innovation Center of Chemical Science and Engineering (Tianjin), School of Materials Science and Engineering, Nankai University, Tianjin 300071, China. Fax: +86 22 2349 9992.

** Corresponding author. State Key Laboratory and Institute of Elemento-Organic Chemistry, Collaborative Innovation Center of Chemical Science and Engineering (Tianjin), School of Materials Science and Engineering, Nankai University, Tianjin 300071, China. Fax: +86 22 2349 9992.

E-mail addresses: xjwan@nankai.edu.cn (X. Wan), yschen99@nankai.edu.cn (Y. Chen).

PCEs around 10% have been achieved [1–3,23–25]. In order to extend the light absorption range, herein, we introduce the DPP unit as the central core, two electron withdrawing groups (octyl cyanoacetate and 3-octyl rhodanine) as end groups and design two small molecules DOR2TDPP and DCAO2TDPP. As expected, the two molecules exhibit broad and red shift solar absorption in contrast to our reported molecules. Initial PCEs of 2.07% and 1.10% were achieved for the molecules DOR2TDPP and DCAO2TDPP based devices with PC₇₁BM as acceptors, respectively.

2. Materials and methods

2.1. Materials

All reactions and manipulations were carried out under argon atmosphere with the use of standard Schlenk techniques. Unless otherwise specified, all the starting materials were purchased from commercial suppliers which were used without any purification. The intermediate M2 was synthesized according to the method we have reported [26].

2.2. Instruments and measurements

Nuclear magnetic resonance (¹H NMR and ¹³C NMR) spectra were taken on a Bruker AV400 Spectrometer. MALDI-TOF spectra were performed on a Bruker Autoflex III instrument. The thermogravimetric analysis (TGA) was carried out on a NETZSCH STA409PC instrument under nitrogen gas flow with a 10 °C min⁻¹ heating rate. UV–Vis spectra were obtained with a JASCO V-570 spectrophotometer. The organic molecule films on quartz used for absorption spectral measurement were prepared by spin-coating their chloroform solutions. X-Ray diffraction (XRD) experiments were performed on a Rigaku D/max-2500 X-ray diffractometer with Cu-K α radiation ($k = 1.5406 \text{ \AA}$) at a generator voltage of 40 kV and a current of 100 mA. Cyclic voltammetry (CV) experiments were performed with a LK98B II microcomputer-based electrochemical analyzer in CH₂Cl₂ solutions which were carried out at room temperature employing a glassy carbon electrode as the working electrode, a saturated calomel electrode (SCE) as the reference electrode, and a Pt wire as the counter electrode. Dichloromethane was distilled from calcium hydride under dry nitrogen immediately prior to use. Tetrabutylammonium phosphorus hexafluoride (Bu₄NPF₆, 0.1 M) in dichloromethane was used as the supporting electrolyte, and the scanning rate was 100 mV s⁻¹.

2.3. Fabrication and characterization of SM-OSCs

The photovoltaic devices were fabricated with a structure of glass/ITO/PEDOT:PSS/Donor:Acceptor/LiF/Al. The ITO coated glass substrates were cleaned by ultrasonic treatment in detergent, deionized water, acetone, and isopropyl alcohol under ultrasonication for 15 min each and dried by a nitrogen blow. PEDOT:PSS layer was spin-coated (3000 rpm, ca. ~40 nm thick) onto the cleaned ITO surface. The substrates were then placed into an argon-filled glove box after being baked at 150 °C for 20 min. Subsequently, the active layer was spin-coated from different blend ratios (weight-to-weight) of donor (8 mg mL⁻¹) and PC₇₁BM in chloroform solution at 1700 rpm for 20 s on the ITO/PEDOT:PSS substrate. The active layer thickness was measured using a Dektak150 profilometer. Finally, a ~1 nm LiF layer and a ~80 nm Al layer were deposited on the active layer under high vacuum (<1.5 × 10⁻⁴ Pa) respectively. The effective area of each cell was 4 mm², defined by masks for all the solar cell devices discussed in this work. The current density–voltage (J–V) curves of the photovoltaic devices

were obtained by a Keithley 2400 source-measure unit. The photocurrent was measured under simulated illumination at 100 mW cm⁻² AM 1.5G irradiation using a xenon-lamp-based solar simulator (Oriel 96000) in an argon filled glove box. The simulator irradiance was calibrated using a certified silicon diode.

2.4. Synthesis

The synthesis routes of DOR2TDPP and DCAO2TDPP are shown in Scheme 1.

2.4.1. Synthesis of compound M1

LDA (2.0 M in hexane, 2.4 ml, 4.8 mmol) was added dropwise to a solution of DPP (1.0 g, 1.9 mmol) in anhydrous tetrahydrofuran (60 ml) at –78 °C under an argon atmosphere, the mixture was stirred for 2 h, then the mixture was stirred at room temperature for 12 h. Afterwards, tri-n-butyltin chloride (1.0 M in THF, 4.8 ml, 4.8 mmol) was added to the mixture at –78 °C and the reaction mixture was stirred for 2 h, then stirred at room temperature for 24 h. The solution was poured into water and the organic phase was extracted with CH₂Cl₂ for three times, and the merged solution was dried with anhydrous sodium sulfate for over 5 h. Solvent was removed by evaporation under vacuum, the product was obtained as dark pink liquid and used in the next step without further purification.

2.4.2. Synthesis of compound M3

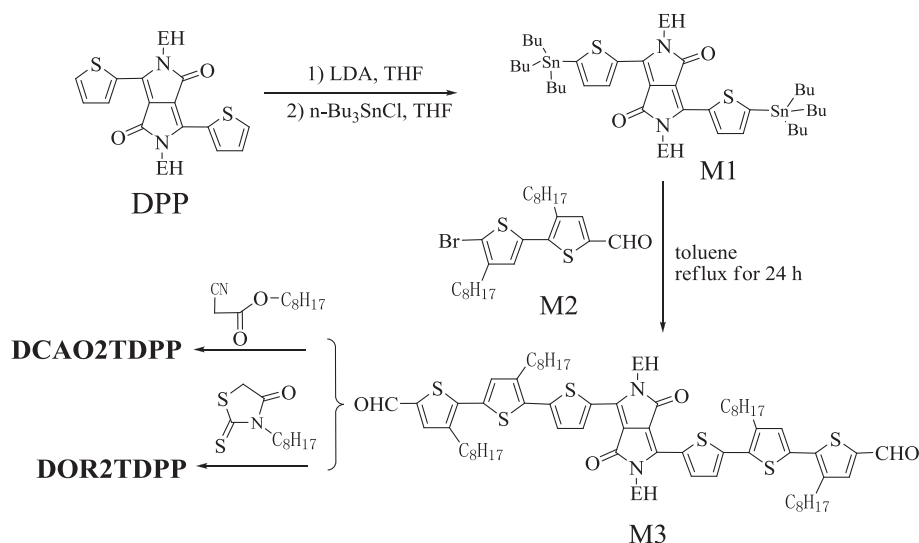
A solution of M2 (2 g, 4.0 mmol) and M1 synthesized above in dry toluene (100 ml) was degassed twice with argon followed by the addition of Pd(PPh₃)₄ (80 mg, 0.06 mmol). After being stirred at 120 °C for 24 h under argon, the reaction mixture was poured into water (100 ml) and extracted with CHCl₃. The organic layer was washed with water for three times, and then dried over Na₂SO₄. After removal of solvent, the crude product was purified by column chromatography on silica gel using a mixture of dichloromethane and petroleum ether (1:3) to afford compound M3 (1.40 g, 56%) as a blue-black solid. ¹H NMR (400 MHz, CDCl₃): δ 9.868 (s, 2H), 9.028 (d, 2H), 7.629 (s, 2H), 7.367 (d, 2H), 7.189 (s, 2H), 4.112 (m, 4H), 2.893 (m, 8H), 1.739 (m, 10H), 1.329 (m, 67H), 0.905 (m, 24H). MS (MALDI-TOF): calculated for C₈₀H₁₁₂N₂O₄S₆ [M]⁺, 1358.14; found, 1359.03.

2.4.3. Synthesis of compound DOR2TDPP

A solution of M3 (500 mg, 0.37 mmol) and 3-octyl rhodanine (900 mg, 3.7 mmol) in dry chloroform was degassed twice with argon followed by the addition of three drops of piperidine. After refluxing for 12 h under argon, the reaction mixture was poured into water (300 ml) and extracted with CHCl₃. The organic layer was washed with water for three times, and then dried over Na₂SO₄. After removal of solvent, the crude product was purified by column chromatography on silica gel using a mixture of dichloromethane and petroleum ether (2:1) to afford compound DOR2TDPP (420 mg, 63%) as a black solid. ¹H NMR (400 MHz, CDCl₃): δ 9.09 (s, 2H), 7.78 (s, 2H), 7.34 (s, 2H), 7.25 (d, 2H), 7.16 (d, 2H), 4.12 (d, 8H), 2.85 (t, 8H), 1.98 (m, 2H), 1.75 (m, 14H), 1.44 (m, 98H), 0.95 (m, 30H). ¹³C NMR (100 MHz, CDCl₃): 201.180, 192.168, 167.504, 141.831, 141.497, 141.057, 139.422, 138.967, 137.301, 136.606, 135.525, 134.630, 134.324, 132.311, 131.547, 130.102, 129.316, 126.824, 124.692, 120.887, 108.459, 44.891, 39.369, 31.880, 31.784, 30.399, 30.218, 29.749, 29.536, 29.431, 29.370, 29.341, 29.284, 29.145, 28.434, 26.997, 26.805, 23.607, 23.174, 22.688, 22.641. MS (MALDI-TOF): calculated for C₁₀₂H₁₄₆N₄O₄S₁₀ [M]⁺, 1811.86; found, 1812.83.

2.4.4. Synthesis of compound DCAO2TDPP

A solution of M3 (500 mg, 0.37 mmol) and doctylcyanoacetate (0.78 ml, 3.7 mmol) in dry chloroform was degassed twice with



Scheme 1. Synthesis routes of DOR2TDPP and DCAO2TDPP.

argon followed by the addition of three drops of triethylamine. After refluxing for 12 h under argon, the reaction mixture was poured into water (300 ml) and extracted with CHCl_3 . The organic layer was washed with water for three times, and then dried over Na_2SO_4 . After removal of solvent, the crude product was purified by column chromatography on silica gel using a mixture of dichloromethane and petroleum ether (3:2) to afford compound DCAO2TDPP (450 mg, 71%) as a black solid. ^1H NMR (400 MHz, CDCl_3): δ 9.08 (s, 2H), 8.23 (s, 2H), 7.60 (s, 2H), 7.36 (d, 2H), 7.24 (d, 2H), 4.32 (t, 4H), 4.09 (d, 4H), 2.87 (t, 8H), 1.96 (m, 2H), 1.76 (m, 14H), 1.33 (m, 96H), 0.90 (m, 30H). ^{13}C NMR (100 MHz, CDCl_3): 249.690, 242.891, 229.693, 219.804, 211.648, 202.937, 190.936, 182.778, 177.839, 163.068, 140.967, 132.038, 130.525, 122.391, 98.024, 66.640, 50.142, 46.133, 42.193, 39.334, 31.794, 30.200, 29.738, 29.514, 29.408, 29.329, 29.271, 29.200, 28.420, 25.822, 23.606, 23.160, 22.688, 14.127, 10.557, MS (MALDI-TOF): calculated for $\text{C}_{102}\text{H}_{146}\text{N}_4\text{O}_6\text{S}_6$ $[\text{M}]^+$, 1715.96; found, 1715.95.

3. Results and discussion

3.1. Thermo-stability

Thermogravimetric analysis (TGA) was used to study the thermo-stability of the two compounds and the TGA curves were shown in Fig. 1. From Fig. 1, we can see that both DOR2TDPP and DCAO2TDPP exhibited good stability with decomposition temperature (T_d) more than 350°C under N_2 atmosphere, indicating good thermo stability for their device application. DCAO2TDPP showed a little better thermal stability than DOR2TDPP since ring-opening reaction might happen when 3-octyl rhodanine end group is exposed to high temperature.

3.2. Optical absorption

The UV–Vis absorption spectra of DOR2TDPP and DCAO2TDPP (in chloroform solution and spin coated film) are shown in Fig. 2. DOR2TDPP and DCAO2TDPP show maximum absorption 631 nm and 629 nm, respectively, in the chloroform solution. Compared with the absorption in solution, film absorption of the two

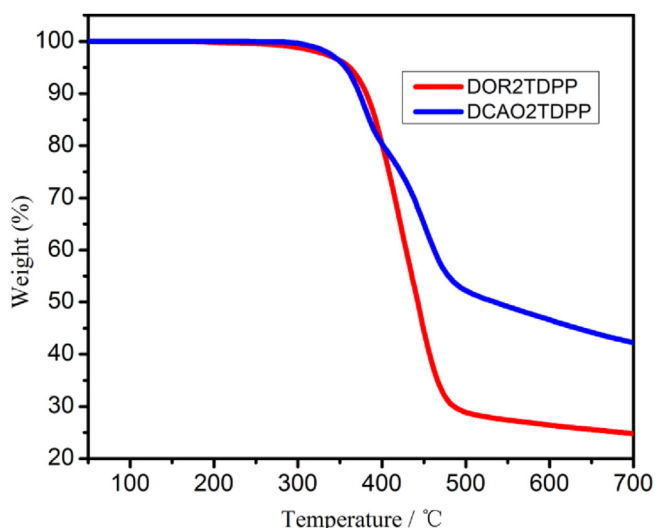


Fig. 1. TGA curves of DOR2TDPP and DCAO2TDPP.

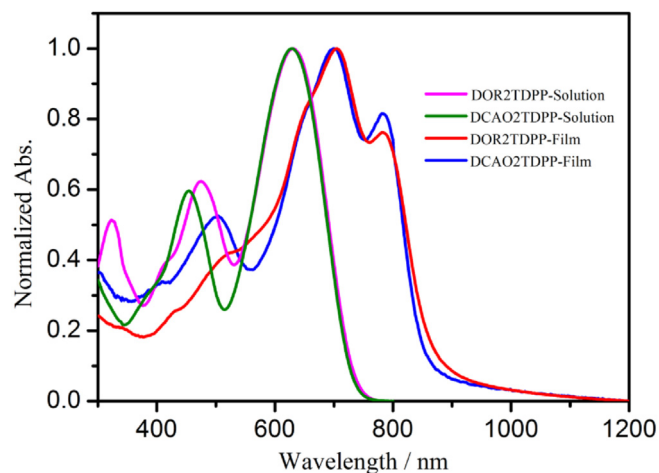


Fig. 2. Absorption spectra of DOR2TDPP and DCAO2TDPP in chloroform solution and films.

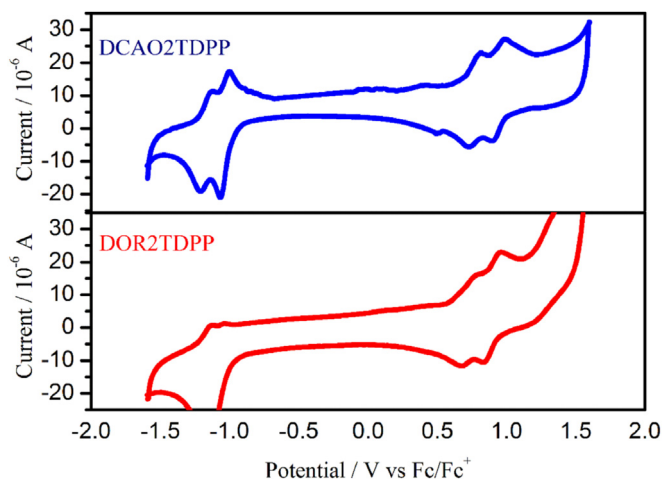


Fig. 3. Cyclic voltammograms of DCAO2TDPP and DOR2TDPP in a dichloromethane solution of $0.1 \text{ mol L}^{-1} \text{ Bu}_4\text{NPF}_6$ with a scan rate of 100 mV S^{-1} on a Pd/C electrode.

compounds exhibit a red shift of about 70 nm, and the maximum absorption peaks were 705 nm for DOR2TDPP and 699 nm for DCAO2TDPP, which all locate in the near infrared region. In contrast to our previous reported A-D-A molecules (D = BDT or oligothiophene), the absorption of DOR2TDPP and DCAO2TDPP showed obvious red shift absorption after introduction of DPP unit as the central core unit.

3.3. Electrochemical properties and electronic energy level

The cyclic voltammetry (CV) was used to study the electrochemical properties of DOR2TDPP and DCAO2TDPP. The potentials were internally calibrated using the ferrocene/ferrocenium (Fc/Fc^+) of the redox couple (4.8 eV below the vacuum level). The energy levels of the HOMO and LUMO are -5.05 eV and -3.27 eV for DOR2TDPP, and -5.12 eV and -3.33 eV for DCAO2TDPP, which were calculated from the onset oxidation potential and the onset reduction potential. The CV curves were shown in Fig. 3, and the detailed values of HOMO, LUMO and bandgaps of the two compounds were listed in Table 1. Calculated from CV curve, the bandgaps (E_g^{CV}) of DOR2TDPP and DCAO2TDPP are 1.78 eV and 1.79 eV, which didn't match with the bandgaps calculated from U–V absorption spectra (E_g^{opt} of DOR2TDPP and DCAO2TDPP are 1.39 eV and 1.40 eV, respectively). For our case, we tested the CV in the corresponding donor dichloromethane solutions. While the optical bandgaps were estimated from the sample solid film absorption. That might be the reason of the inconsistency of the bandgap values from CV and absorption.

In order to further investigate the electronic and optical properties of these two DPP based molecules, we performed molecular geometry optimization using density functional theory (DFT) calculation (B3LYP/6-31G*), and frequency analysis was followed that the obtained optimized structures were in stable states. The optimized molecular geometries and frontier molecular orbitals of DOR2TDPP and DCAO2TDPP were shown in Figs. S7–9. Time-dependent DFT (TDDFT) calculation of the S0–S1 transitions were

Table 1

Optical and electrochemical data of compound DOR2TDPP and DCAO2TDPP.

Compounds	λ_{max} solution/nm	λ_{max} film/nm	E_g^{opt} /eV	E_g^{CV} /eV	HOMO/eV	LUMO/eV
DOR2TDPP	631	705 & 785	1.39	1.78	-5.05	-3.27
DCAO2TDPP	629	699 & 782	1.40	1.79	-5.12	-3.33

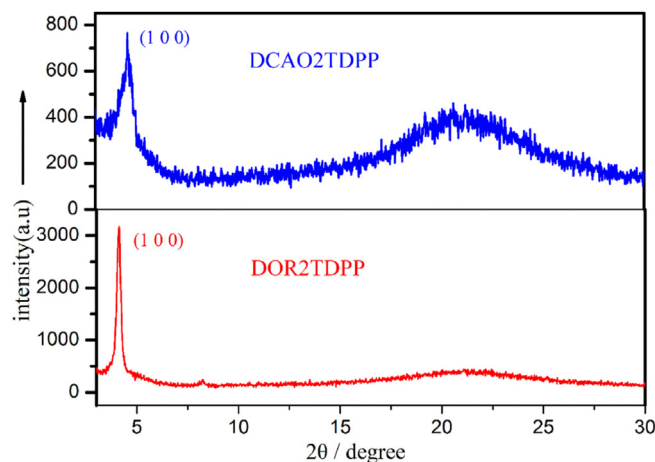


Fig. 4. XRD patterns of DCAO2TDPP and DOR2TDPP films spin-coated from CHCl_3 onto glass substrate.

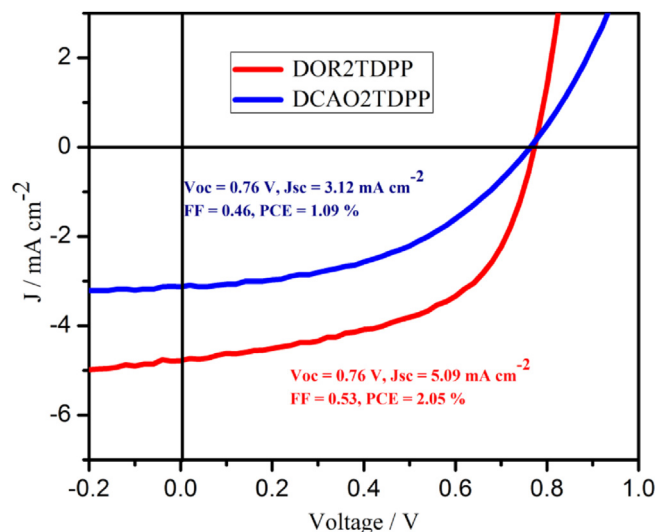


Fig. 5. Current density–voltage characteristics of the OSC devices based on DOR2TDPP and DCAO2TDPP.

then performed on basis of optimized geometries in the ground states, to investigate the vertical excitation energies by analyzing the lowest 30 singlet roots of the nonhermitian eigenvalue equations. The calculation results were summarized in Tables S1–2, and the simulated UV–vis spectra were shown in Fig. S10. The calculation results are similar to the experimental results and the maximum absorption bands mainly correspond to pure HOMO–LUMO transition with π – π^* character.

3.4. X-ray diffraction (XRD)

X-Ray diffraction analysis was used to investigate the crystallinity of the two molecules and the patterns were shown in Fig. 4.

Table 2

Influence of D/A ratio on the performance of the SM-OPVs based on DCAO2TDPP and DOR2TDPP.

Compound	Blend ratio (D:A)	V_{oc}/V	$J_{sc}/\text{mA cm}^{-2}$	FF	PCE (%)
DCAO2TDPP	1:0.5	0.76	1.60	0.32	0.38
	1:0.8	0.77	1.49	0.26	0.29
	1:1	0.77	2.44	0.41	0.77
DOR2TDPP	1:1.2	0.77	2.10	0.40	0.64
	1:0.5	0.75	3.91	0.48	1.40
	1:0.8	0.74	4.32	0.47	1.50
	1:1	0.74	5.11	0.45	1.70
	1:1.2	0.77	4.01	0.53	1.63

Table 3

Influence of amount of DIO on the performance of the SM-OPVs based on DCAO2TDPP and DOR2TDPP with D/A = 1:1.

Compound	DIO (%)	V_{oc}/V	$J_{sc}/\text{mA cm}^{-2}$	FF	PCE (%)
DCAO2TDPP	1	0.77	2.55	0.39	0.76
	3	0.76	3.12	0.46	1.09
	5	0.75	1.79	0.40	0.53
DOR2TDPP	1	0.75	4.82	0.53	1.91
	3	0.76	5.09	0.53	2.05
	5	0.76	4.39	0.52	1.73

From Fig. 4, we can see that a strong reflection peak (100) at $2\theta = 4.12^\circ$ was observed for DOR2TDPP, corresponding to a d_{100} -spacing values of 18.7 Å. While the reflection peak (100) of DCAO2TDPP at $2\theta = 4.56^\circ$ (corresponding to a d_{100} -spacing values of 20.7 Å) was much weaker comparing with that of DOR2TDPP, indicating that the DOR2TDPP had more ordered packing behavior than DCAO2TDPP.

3.5. Photovoltaic performance

Solution processed OSCs with a bulk-heterojunction structure were fabricated using the two compounds as donor and PC₇₁BM as

acceptor. The device structure is glass/ITO/PEDOT:PSS/active layer/LiF/Al. The device performance was optimized by adjusting the blend ratio of donor versus acceptor and varying the amount of additive (1, 8-Diiodooctane, DIO). The optimized typical current density-voltage ($J-V$) curves of devices were shown in Fig. 5 and the results were summarized in Tables 2 and 3. For both of DOR2TDPP and DCAO2TDPP based OSCs, the best performance was obtained from the device with a blend ratio of 1:1 together with 3% DIO, which gave a V_{oc} of 0.76 V, a J_{sc} of 5.09 mA cm^{-2} , a FF of 0.53 and a PCE of 2.05% for DOR2TDPP, and a V_{oc} of 0.76 V, a J_{sc} of 3.12 mA cm^{-2} , a FF of 0.46 and a PCE of 1.09% for DCAO2TDPP, respectively.

Atomic force microscopy (AFM) was applied to study the morphology of the films with different ratio of DIO. As shown in Fig. 6, we can see that the two molecules blending films showed much different morphologies when different ratio of DIO were added. For the blending film DOR2TDPP:PCBM, when 3% DIO was added, the root-mean-squared (RMS) roughness was 7.06 nm, which is lower than that of films with 1% (7.76 nm) and 5% DIO (12.4 nm). Also, the films with 1% and 5% DIO also showed much large phase separation in contrast with the film with 3% DIO. For the blending film DCAO2TDPP:PCBM, when 1% DIO was added, a large phase separation was observed with roughness 12.6 nm. The surface became relatively smoother with RMS roughness of 7.05 nm when 3% DIO was added. When 5% DIO was added, the blending film roughness increased to 11.9 nm. There were no obvious interpenetrating structures in the DCAO2TDPP:PCBM blending film and there existed large phase separation when different ratio DIO was added, which is responsible for the poor devices performances of DCAO2TDPP:PCBM devices.

To further investigate the device performance, the external quantum efficiency (EQE) of the two molecules based devices was measured as shown in Fig. 7. From the curves, we can see that the DOR2TDPP and DCAO2TDPP based devices show broad absorption, however, the EQE values are very low (below 30%), especially, the EQE values are below 10% from 700 nm to 900 nm. The low EQE values indicate that the photo-response of the two molecules is not

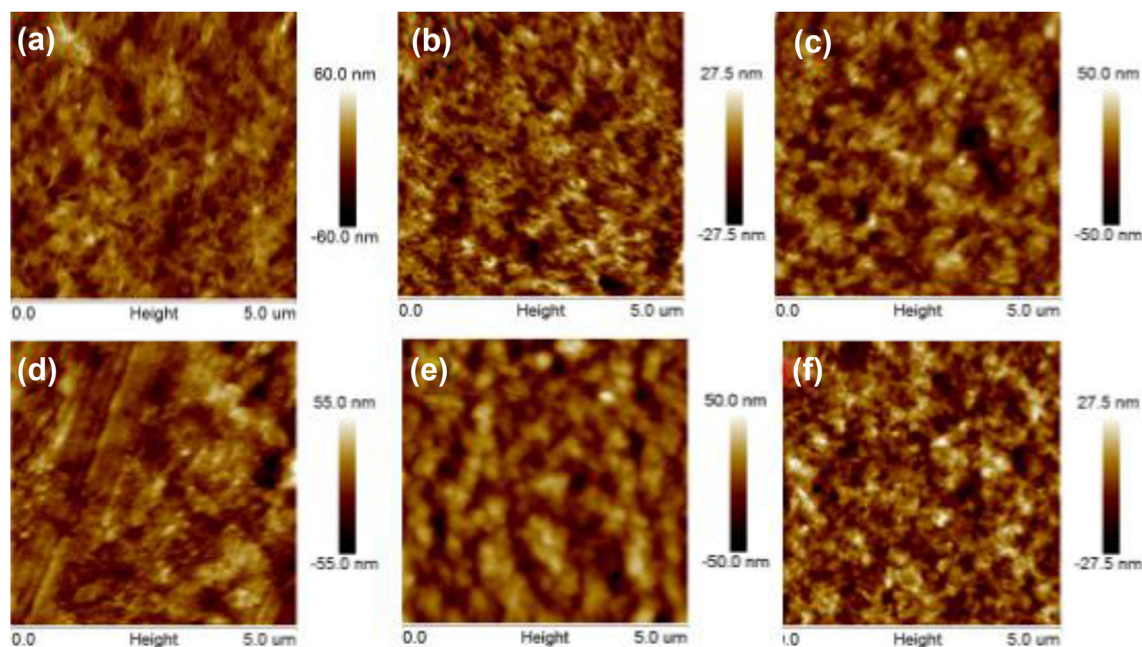


Fig. 6. AFM images of Donor: PC₇₁BM films spin-coated from their chloroform solution at a weight ratio of 1:1, (a) DOR2TDPP: PC₇₁BM with 1% DIO, (b) DOR2TDPP: PC₇₁BM with 3% DIO, (c) DOR2TDPP: PC₇₁BM with 5% DIO, (d) DCAO2TDPP: PC₇₁BM with 1% DIO, (e) DCAO2TDPP: PC₇₁BM with 3% DIO, (f) DCAO2TDPP: PC₇₁BM with 5% DIO.

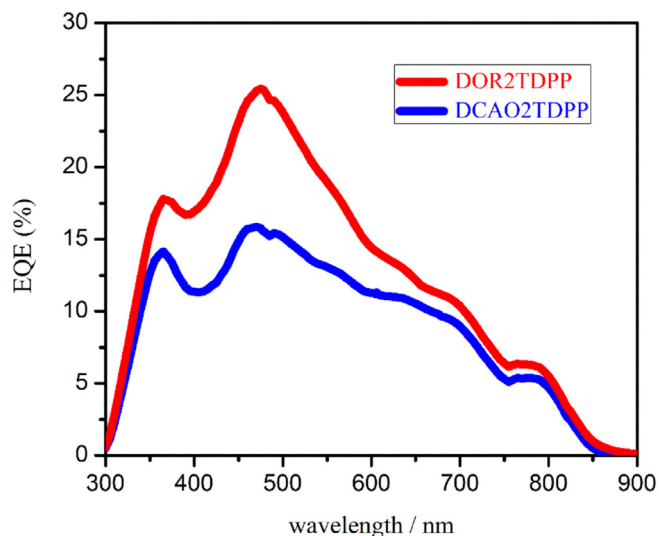


Fig. 7. EQE curves for both devices based on DOR2TDPP and DCAO2TDPP.

efficient enough to change photons into charge carriers. Though both of the two molecules have broad absorption from ultraviolet to near infrared, the solar light cannot be transformed to electric energy efficiently, especially the near infrared light. The energy of the excitons excited by the near infrared light may be relatively lower than that of excitons visible light excited, and could not separate effectively, then bimolecular combination occurred and finally resulted in low J_{sc} .

4. Conclusion

In conclusion, two new small molecules with a DPP core were designed and synthesized for solution-processed small molecule organic solar cells. As expected, both of the two molecules have a broad and red shifted absorption compared with that of the molecules our group synthesized before. However, the devices performances were poor owing to the large domain size and phase separation. Although the morphologies could be tuned through various strategies such as additive, thermal annealing and etc., the intrinsic properties, especially the intrinsic packing behaviors are needed to further be investigated, which play a great role on the morphology forming. Thus, it is still a challenge to design molecules which could meet all the demands of high photovoltaic devices.

Acknowledgment

The authors gratefully acknowledge financial support from the MOST (Grants 2014CB643502), NSFC (Grants 91433101, 51422304, and 51373078), NSF of Tianjin City (Grant 13RCGFGX01121), and PCSIRT (IRT1257).

Appendix A. Supplementary data

Supplementary data related to this article can be found at <http://dx.doi.org/10.1016/j.dyepig.2015.11.024>.

References

- [1] Zhang Q, Kan B, Liu F, Long GK, Wan XJ, Chen XQ, et al. Small-molecule solar cells with efficiency over 9%. *Nat Phot* 2015;9:35–41.
- [2] Kan B, Zhang Q, Li MM, Wan XJ, Ni W, Long GK, et al. Solution-processed organic solar cells based on dialkylthio substituted benzodithiophene unit with efficiency near 10%. *J Am Chem Soc* 2014;136:15529–32.
- [3] Kan B, Li MM, Zhang Q, Liu F, Wan XJ, Wang YC, et al. A series of simple oligomer-like small molecules based on oligothiophenes for solution-processed solar cells with high efficiency. *J Am Chem Soc* 2015;137:3886–93.
- [4] Liu YH, Zhao JB, Li ZK, Mu C, Hu HW, Jiang K, et al. Aggregation and morphology control enables multiple cases of high-efficiency polymer solar cells. *NatComm* 2014;5:5293.
- [5] Kong J, Hwang IW, Lee K. Top-Down approach for nanophase reconstruction in bulk heterojunction solar cells. *Adv Mater* 2014;26:6275–83.
- [6] Chen JD, Cui CH, Li YQ, Zhou L, Ou QD, Li C, et al. Single-junction polymer solar cells exceeding 10% power conversion efficiency. *Adv Mater* 2015;27:1035–41.
- [7] Liu C, Yi C, Wang K, Yang YL, Bhatta RS, Tsige M, et al. Single-junction polymer solar cells with over 10% efficiency by a novel two-dimensional donor–acceptor conjugated copolymer. *ACS Appl Mater Interface* 2015;7:4928–35.
- [8] He ZC, Xiao B, Liu F, Wu HB, Yang YL, Xiao S, et al. Single-junction polymer solar cells with high efficiency and photovoltage. *Nat Phot* 2015;9:174–9.
- [9] Kim J, Hong ZR, Li G, Song TB, Chey J, Lee YS, et al. 10.5 % efficient polymer and amorphous silicon tandem photovoltaic cell. *Nat Comm* 2015;6:6391.
- [10] Ouyang XH, Peng RX, Ai L, Zhang XY, Ge ZY. Efficient polymer solar cells employing a non-conjugated small-molecule electrolyte. *Nat Phot* 2015;9:520–4.
- [11] Zhang JQ, Zhang YJ, Fang J, Lu K, Wang ZY, Ma W, et al. Conjugated polymer–small molecule alloy leads to high efficient ternary organic solar cells. *J Am Chem Soc* 2015;137:8176–83.
- [12] Lee JK, Ma WL, Brabec CJ, Yuen J, Moon JS, Kim JY, Lee K, Bazan GC, et al. Processing additives for improved efficiency from bulk heterojunction solar cell. *J Am Chem Soc* 2008;130:3619–23.
- [13] Yao Y, Hou JH, Xu Z, Li G, Yang Y. Effect of solvent mixtures on the nanoscale phase separation in polymer solar cells. *Adv Funct Mater* 2008;18:1783–9.
- [14] Hoven CV, Dang XD, Coffin RC, Peet J, Nguyen TQ, Bazan GC. Improved performance of polymer bulk heterojunction solar cells through the reduction of phase separation via solvent additives. *Adv Mater* 2010;22:E63–6.
- [15] Zhao GJ, Zhao YJ, Li YF. 6.5 % efficiency of polymer solar cells based on poly(3-hexylthiophene) and indene-C₆₀ bisadduct by device optimization. *Adv Mater* 2010;22:4355–8.
- [16] Li G, Yao Y, Yang HC, Shrotriya V, Yang G, Yang Y. “Solvent annealing” effect in polymer solar cells based on poly(3-hexylthiophene) and methanofullerenes. *Adv Funct Mater* 2007;17:1636–44.
- [17] Miller S, Fanchini G, Lin YY, Li C, Chen CW, Su WF, et al. Investigation of nanoscale morphological changes in organic photovoltaics during solvent vapor annealing. *J Mater Chem* 2008;18:306–12.
- [18] Wang K, Yi C, Hu XW, Liu C, Sun Y, Hou JH, et al. Enhanced performance of polymer solar cells using PEDOT: PSS doped with Fe₃O₄ magnetic nanoparticles aligned by an external magnetostatic field as an anode buffer layer. *ACS Appl Mater Interfaces* 2014;6:13201–8.
- [19] Ha DH, Fang ZQ, Hu LB, Munday JN. Paper-based anti-reflection coatings for photovoltaics. *Adv Energy Mater* 2014;4:1301804.
- [20] Chen JD, Zhou L, Ou QD, Li YQ, Shen S, Lee ST, et al. Enhanced light harvesting in organic solar cells featuring a biomimetic active layer and a self-cleaning antireflective coating. *Adv Energy Mater* 2014;4:1301777.
- [21] Walker B, Tomayo AB, Dang XD, Zalar P, Seo JH, Garcia A, et al. Nanoscale phase separation and high photovoltaic efficiency in solution-processed, small-molecule bulk heterojunction solar cells. *Adv Funct Mater* 2009;19:3063–9.
- [22] Qu SY, Tian H. Diketopyrrolopyrrole (DPP)-based materials for organic photovoltaics. *Chem Commun* 2012;48:3039–51.
- [23] Chen YS, Wan XJ, Long GK. High performance photovoltaic applications using solution processed small molecules. *Acc Chem Res* 2014;46:2645–55.
- [24] Ni W, Li MM, Wan XJ, Zuo Y, Kan B, Feng HR, et al. A new oligobenzodithiophene end-capped with 3-ethyl-rhodanine groups for organic solar cells with high open-circuit voltage. *Sci Chin Chem* 2015;58:339–46.
- [25] Li MM, Ni W, Feng HR, Kan B, Wan XJ, Zhang YM, et al. Dithienopyrrole based small molecule with low band gap for organic solar cells. *Chin J Chem* 2015;33:852–8.
- [26] Liu YS, Wan XJ, Wang F, Zhou JY, Long GK, Tian JG, et al. High-performance solar cells using a solution-processed small molecule containing benzodithiophene Unit. *Adv Mater* 2011;23:5387–91.